Biophysical Journal, Volume *110*

Supplemental Information

Free-Energy Landscape of the Amino-Terminal Fragment of Huntingtin in Aqueous Solution

Vincent Binette, Sébastien Côté, and Normand Mousseau

Supporting Material – Free energy Landscape of the Amino-terminal Fragment of Huntingtin in Aqueous Solution

Vincent Binette[△], Sébastien Côté[△,*], and Normand Mousseau[*]

Département de Physique and Groupe de recherche sur les protéines membranaires (GEPROM), Université de Montréal, C.P. 6128, succursale Centre-ville, Montréal (Québec), Canada

HREXMetaD on Htt17_coil

We perform a second HREXMetaD simulation on Htt17 starting from a random coil state (Htt17_coil) to assess the robustness of our simulations starting from the NMR model obtained in the presence of DPC micelles (Htt17_nmr). Both systems have the same size and number of water molecules. Both simulations are run at 303K using 16 scales spanning 1.0 to 0.3 with the same intermediate scales. Exchanges between neighboring scales are attempted every 4 ps resulting in an exchange rate of about 20–40%.

The free energy surfaces (FES) in terms of S_α and S_{gyr} for these two simulations indicate that the main features and the extend of the basin are very similar in both simulation sets (compare Figure S1 on Htt17_nmr to Figure S4 on Htt17_coil). The global α-helix probability is also similar: 29.3 $\pm$ 0.7% for Htt17_nmr and 26.9 $\pm$ 0.3% for Htt17_coil. While residues 7 to 12 are less structured in Htt17_coil, the main features of the per residue secondary structure are also preserved: moderate helical content for the first residues, presence of a turn between residues 10 and 13 and more disordered for the last residues (Figure S9). The FES in terms of the number of helical H-bonds (horizontal axis, S_α) and the gyration radius (vertical axis, S_{rg}) displays a similar conformational ensemble characterized by two main structures: two-helix bundle structures (clusters 1,2,4,5), with the first half of the peptide more structured than the second half (cluster 1,4) and almost fully random structures (clusters 3) as shown in Figure S9. Both kinds of structures were also identified in the simulation Htt17_nmr. The FES in terms of the number of helical H-bonds (S_α) and the solvent accessible surface area (SASA) of Htt17's non-polar residues is also similar in both cases as most of the structural ensemble is located between 3 and 5 nm^2 (data not shown). Finally, the contact maps show that the key non-polar and electrostatic contacts are preserved: Met8–Phe17 (24.1% for Htt17_nmr vs. 26.8% for Htt17_coil), Glu5–Lys9 (50.3% for Htt17_nmr vs. 44.5% for Htt17_coil), Glu12–Lys9 (42.3% for Htt17_nmr vs. 38.2% for Htt17_coil), and Glu12–Lys15 (64.0% for Htt17_nmr vs. 58.5 for Htt17_coil) (data not shown).

Overall, we observe an excellent agreement between these two simulations that start from the two very different initial states indicating adequate convergence assessment and sampling of the conformational ensemble.

HREXMetaD vs. PTMetaD for Htt17

In addition to our HREXMetaD simulation on Htt17, we use a second methodology that is very popular – parallel tempering metadynamics (PTMetaD) – to compute the free energy surface of Htt17 in terms of S_α and S_{gyr}. Parallel tempering is often used on its own to simulate protein folding because it increases the probability of escaping free energy minima by allowing exchanges between simultaneous MD simulations at different temperatures (1, 2). Similarly to HREXMetaD, the combination of MetaD and PT dumbed PTMetaD allows one to correctly sample other CVs not explicitly taken into account by the time-dependent biased potential as demonstrated from proteins with similar conformational ensemble to Htt17 (3–5). The temperature distribution used for PT spans 278 to 646K and the intermediate temperatures are determined using a recent protocol and requiring an exchange rate of approximately 20% for a total of 64 replicas (6).

The free energy surface in terms of the number of helical H-bonds (S_α) and gyration radius (S_{gyr}) obtained using PTMetaD is shown in Figure S10. We observe that its extent is very similar to that obtained using HREXMetaD (Figure S9), while there are two minor differences: (i) the FES minimum is now bounded between 3 and 6 helical H-bonds – instead of between 2 and 6 for the HREXMetaD simulations – and has narrower gyration radius bracket and (ii) the fully random structures are slightly less favored when using PTMetaD.

0006-3495/08/09/2624/12 $2.00 doi:

Even if these changes in the FES lead to a slight increase of the α-helical propensity from 29.3 $\pm$ 0.7% (HREXMetaD) to 38$\pm$ 3% (PT-MetaD), the main features of the per residue secondary structure profile are unchanged with the first half of the peptide being more structured than the second half (compare Figures S9 and S10). From the same Figures, the cluster analysis of the structures sampled in the FES minima (below 5 kJ/mol) further indicates that our HREXMetaD and PTMetaD simulations sample a similar structural ensemble. Indeed, in agreement with our HREXMetaD simulations, we see that Htt17 mostly adopts a two-helix bundle structure (see clusters 1,2 and 4).

The good agreement between our PTMetaD and HREXMetaD simulations demonstrates the robustness of the sampling in both methodologies although we believe that HREX might escape local minima faster than PT because the configurations have significantly less replicas to diffuse in. The use of HREXMetaD might then reduce the probability that MetaD adds wrong biases to the free energy landscape when compared to PTMetaD.

Comparison to the solution NMR experiment on Htt17

With large intensities for H^{α}(i)-H^{N}(i+1) NOEs, medium intensities for H^{α}(i)-H^{N}(i) NOEs and very small ones for medium range NOEs, the structural ensemble sampled during our simulations is largely compatible with the NMR experiment on Htt17 in aqueous solution indicating that it is mostly unstructured in solution (7) (Figure S11).

We refine our analysis by comparing the interproton NOEs for our most scaled replica (replica 16) to our unscaled replica (replica 1) that populate a very different conformational ensemble : the helix propensity is only 3.3 $\pm$ 0.1% for the most scaled replica, while it is 36.9 $\pm$ 0.9% for the unscaled replica. We find an almost identical trend for H^{α}(i)-H^{N}(i) interproton distances, slightly weaker H^{N}(i)-H^{N}(i+1) and H^{α}(i)-H^{N}(i+2) intensities, and stronger H^{α}(i)-H^{N}(i+1) intensities (Figure S11). For its part, the medium-range H^{α}(i)-H^{N}(i+3) NOEs are weaker (data not shown). Taken together, this indicates that the structural ensemble in terms of NOEs of the unscaled replica is dominated by mostly random conformations as the H^{α}(i)-H^{N}(i+1) intensities are very large with a small population of helical conformations as the H^{α}(i)-H^{N}(i+2) and H^{α}(i)-H^{N}(i+3) intensities are stronger compared to the most scaled replica.

We also compute the interproton NOE intensities for two extreme cases: a perfect α-helix and a completely extended conformation. The perfect" conformations are build with PYMOL and then minimized with the conjugate gradient method to avoid structural clashes. The results are shown in Figure S11. Comparing with both sets, we conclude the intensities observed are consistent with mostly disordered structures.

We note, moreover that we find very low H^{N}(i)-H^{N}(i+1) intensities (below 0.05) except for two residues where the intensities drastically increase to 0.7 indicating that only small structural changes can lead to large fluctuations of this NOE.

Overall, our investigation of the interproton distances shows a globally good agreement between our simulations and NMR experiments. Indeed, three out of four interproton distances are well conserved with large H^{α}(i)-H^{N}(i+1), medium H^{α}(i)-H^{N}(i) and very small H^{α}(i)-H^{N}(i+2) intensities. We find high intensities for the H^{N}(i)-H^{N}(i+1) NOEs, which seems conflicting with the NMR experiment showing very weak intensities. The lack of sequential H^{N}(i)-H^{N}(i+1) NOE in the NMR experiment is an indicator of a mostly disorder structural ensemble.A more thorough examination of our simulations leads us to believe that the difference is due only to very small and local structural changes as both the fully extended conformation and the structural ensemble sampled by the most scaled replica (having only 3.3 $\pm$ 0.1% of helical content) have H^{N}(i)-H^{N}(i+1) intensities of 0.7 and higher. The presence of H^{α}(i)-H^{N}(i+3) NOEs indicates a small population of helical structures, not found in NMR experiments. We thus conclude that structural ensemble of Htt17 is, at the exception of very local flexibility and small overestimation of the helical content, in agreement with this experiment.

Particle-Mesh Ewald vs. Generalized reaction field

Long-range electrostatic calculation computed using Particle-Mesh Ewald (PME) can, in some cases, artificially increase the α-helical content of peptides possessing an α-helical propensity (8). To probe the magnitude of this effect on our system, we redid a simulation for the Htt17(2LD2) system and replaced the PME calculation by a Generalized Reaction Field (GRF).

The resulting two-dimensional FES shows a single large minimun bounded by between 2 and 6 helical H-bonds and a gyration radius between 0.6 and 0.8 nm S12. Comparison with the same simulation done with PME shows that the use of the GRF does not alter the position of the free energy minima. However, the conformations with more than 6 helical H-bonds are slightly destabilized as the free energy slowly increases with the number of helical H-bonds compared to its PME counterpart. A more detailed analysis of the secondary structure reveals that the GRF reduces the α-helical content passing from 29.7 $\pm$ 0.7% with PME to 17 $\pm$ 4%. The per residue secondary structure profile is entirely conserved during the process with the first half of the peptide being more structured than the second one. In both simulation, we observe a mix of two-helix, single helix, helix/coil and coil conformations.

Overall, the results of this simulation indicate that GRF slightly destabilizes the α-helix in our system. The secondary structure per residue profiles of both simulations are nonetheless in very good agreement and we conclude that the GRF and PME scheme show coherent qualitative behavior for Htt17.

Probing the effects of revised proline parameters

In order to probe more meticulously the effect of the poly-proline domain, we simulated Htt17$Q_{17}P_{11}$ using a recent version of the AMBER99sb*-ILDN forcefield that includes revised proline parameters (AMBER99sb*-ILDNP), derived from fitting experimental correlation times and NMR J couplings (9).

The newly obtained FES shows two main minima, the first one characterized by a set of states with 7 to 10 helical H-bonds and a gyration radius of 0.8 nm and a second one characterized by around 6 helical H-bonds and a gyration radius slightly lower than 1.0 nm (see Figure S13). Both these regions are also very stable in the simulation using the AMBER99sb*-ILDN forcefield. The main discrepancy between both FES is the decrease of stability of the fully formed α-helix (more than 12 helical H-bonds) by about 6.5 kJ/mol.

In more details, the resulting secondary structure per residue profile is presented in Figure S13. The Htt17 and Q_{17} domain are characterized respectively by 66 $\pm$ 11% and 18 $\pm$ 7% of α-helical content. Those results indicate that revised proline parameters slightly reduce the α-helical content of the Htt17 domain (from 70 $\pm$ 2% to 66 $\pm$ 11%) but decrease the α-helical content of the Q_{17} domain (from 45 $\pm$ 3% to 18 $\pm$ 7%). Despite the decrease of the helical content, the qualitative behavior of secondary structure per residue profile is well preserved between the two forcefield. Indeed, with both forcefield, Htt17 adopts an helical conformation that is maintained throughout the first few glutamines and the helical propensity slowly decreases toward the P_{11} domain which forms a PPII-helix. In term of structure, a cluster analysis of the structure found inside the FES minima (below 8kJ/mol) reveals that the most populated cluster depicts Htt17 as an α-helix between residues 3 and 16 and the Q_17 is entirely unstructured. Htt17 non-polar residues are mostly accessible to the solvent, in agreement with the simulations done with AMBER99sb*-ILDN.

In summary, the revised proline parameters do not cause drastic changes of structure for both the Htt17 and P_{11} domain. Indeed, Htt17 is still mostly helical with a very similar secondary structure profile, although the fully formed helix is less present. The P_{11} domain, for its part, maintain the PPII-helix. The main difference causes by the new forcefield is on the the Q_{17} domain which is now less structured.

References

1. Hansmann, U. H. E., 1997. Parallel tempering algorithm for conformational studies of biological molecules. Chem. Phys. Lett. 281:140–150.
2. Sugita, Y., and Y. Okamoto, 1999. Replica-exchange molecular dynamics method for protein folding. Chem. Phys. Lett. 314:141–151.
3. Barducci, A., M. Bonomi, and P. Derreumaux, 2011. Assessing the quality of the OPEP coarse-grained force field. J. Chem. Theory Comput. 7:1928–1934.
4. Camilloni, C., D. Schaal, K. Schweimer, S. Schwarzinger, and A. De Simone, 2012. Energy landscape of the prion protein helix 1 probed by metadynamics and NMR. Biophys. J. 102:158–167.
5. Camilloni, C., D. Provasi, G. Tiana, and R. A. Broglia, 2008. Exploring the protein G helix free-energy surface by solute tempering metadynamics. Proteins 71:1647–1654.
6. Prakash, M. K., A. Barducci, and M. Parrinello, 2011. Replica temperatures for uniform exchange and efficient roundtrip times in explicit solvent parallel tempering simulations. J. Chem. Theory Comput. 7:2025–2027.
7. Thakur, A. K., M. Jayaraman, R. Mishra, M. Thakur, V. M. Chellgren, I.-J. L. Byeon, D. H. Anjum, R. Kodali, T. P. Creamer, J. F. Conway, A. M. Gronenborn, and R. Wetzel, 2009. Polyglutamine disruption of the huntingtin exon 1 N terminus triggers a complex aggregation mechanism. Nat. Struct. Mol. Biol. 16:380–389.
8. Weber, W., P. H. Hünenberger, and J. A. McCammon, 2000. Molecular dynamics simulations of a polyalanine octapeptide under Ewald boundary conditions: influence of artificial periodicity on peptide conformation. The Journal of Physical Chemistry B 104:3668–3675.
9. Aliev, A. E., M. Kulke, H. S. Khaneja, V. Chudasama, T. D. Sheppard, and R. M. Lanigan, 2014. Motional timescale predictions by molecular dynamics simulations: Case study using proline and hydroxyproline sidechain dynamics. Proteins: Structure, Function, and Bioinformatics 82:195–215.

Supporting Figures

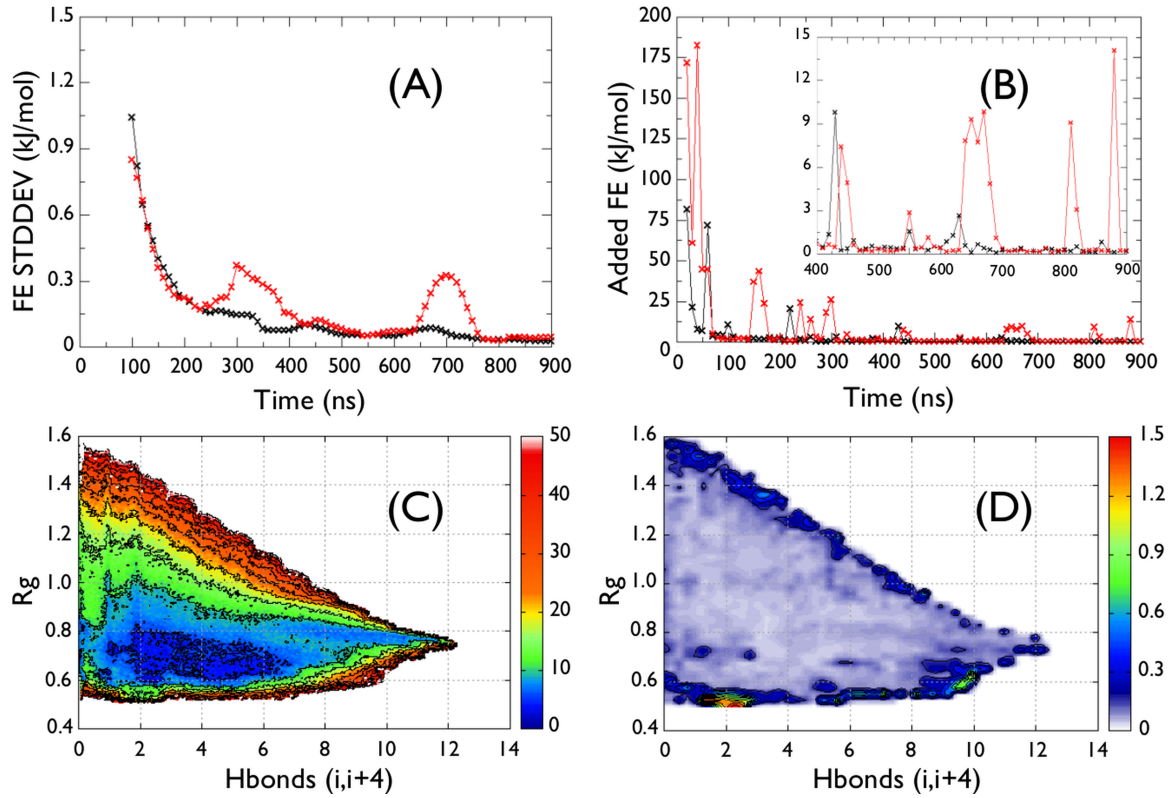

Figure S1: Convergence assessment of the Htt17_nmr simulation. **(A)** Running average of the standard deviation of the 1D-FES (S_α in black and S_{gyr} in red) over 100 ns time-windows. **(B)** Total addition of free energy to the FES every 10 ns. **(C)** The 2D-FES (S_α;S_{gyr}) and **(D)** its uncertainty computed on the convergence interval (400–900 ns), which is determined from the small modifications of the FES after 400 ns shown in (A) and (B). We observe that the uncertainty on the FES is mostly located to its border, while it is low (< 0.5 kJ/mol) inside the basin. Energy isolines are drawn every 5 kJ/mol for **(C)** and 0.15 kJ/mol for **(D)**.

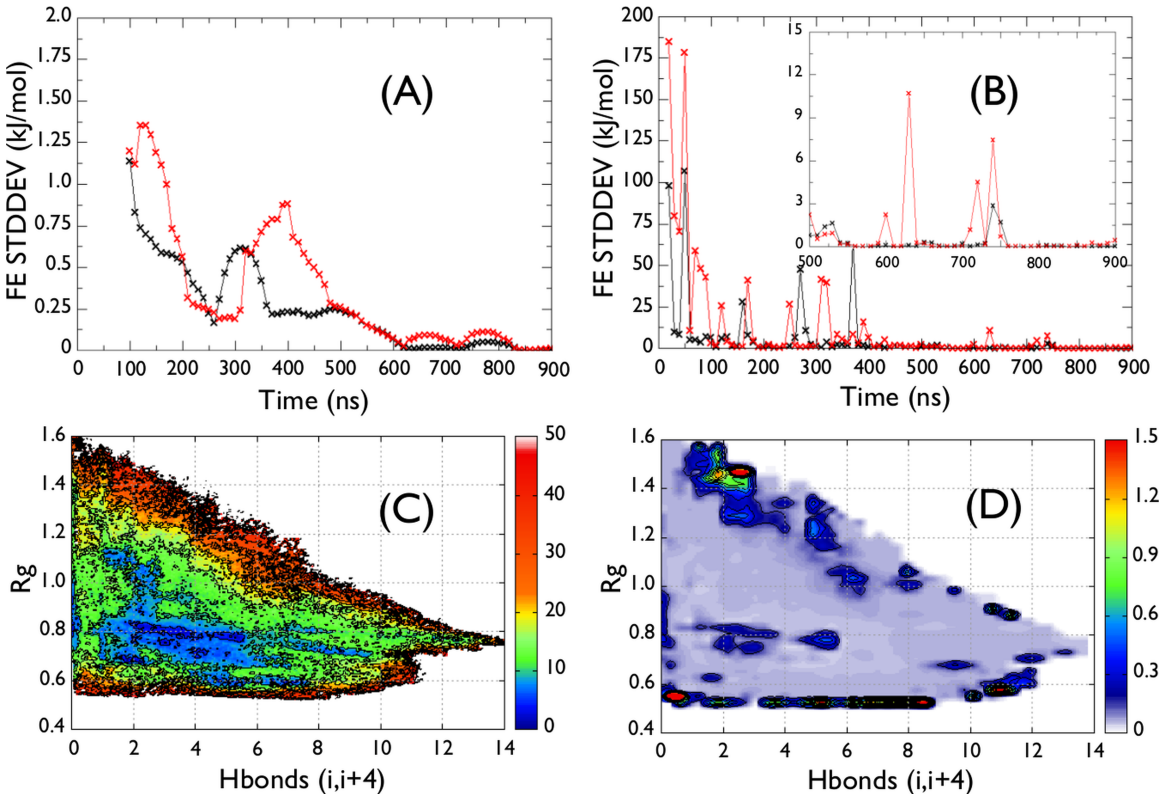

Figure S2: Convergence assessment of the Htt17Q_{17} simulation. **(A)** Running average of the standard deviation of the 1D-FES (S_α in black and S_{gyr} in red) over 100 ns time-windows. **(B)** Total addition of free energy to the FES every 10 ns. **(C)** The 2D-FES (S_α;S_{gyr}) and **(D)** its uncertainty computed on the convergence interval (500–900 ns), which is determined from the small modifications of the FES after 500 ns shown in (A) and (B). We observe that the uncertainty on the FES is mostly located to its border, while it is low (< 1.0 kJ/mol) inside the basin. Energy isolines are drawn every 5 kJ/mol for **(C)** and 0.15 kJ/mol for **(D)**.

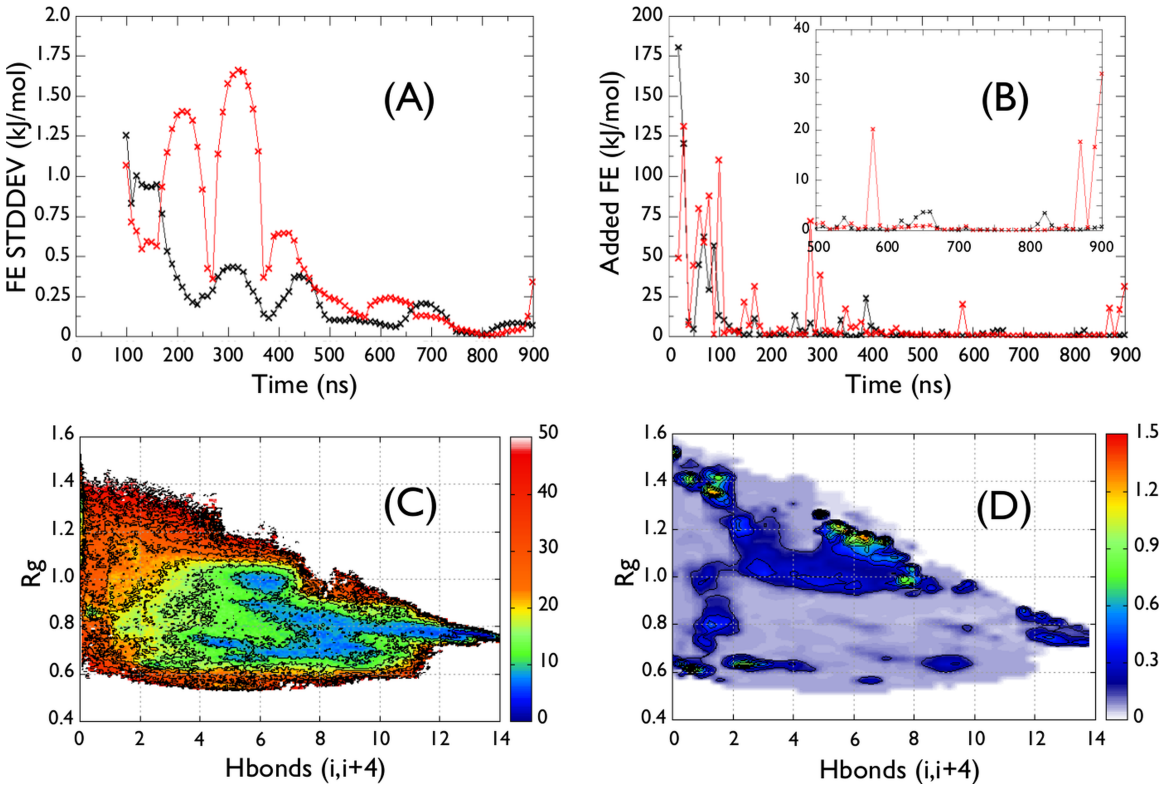

Figure S3: Convergence assessment of the Htt17$Q_{17}P_{11}$ simulation. **(A)** Running average of the standard deviation of the 1D-FES (S_α in black and S_{gyr} in red) over 100 ns time-windows. **(B)** Total addition of free energy to the FES every 10 ns. **(C)** The 2D-FES (S_α;S_{gyr}) and **(D)** its uncertainty computed on the convergence interval (500–900 ns), which is determined from the small modifications of the FES after 500 ns shown in (A) and (B). We observe that the uncertainty on the FES is mostly located to its border, while it is low (< 1.0 kJ/mol) inside the basin. Energy isolines are drawn every 5 kJ/mol for **(C)** and 0.15 kJ/mol for **(D)**.

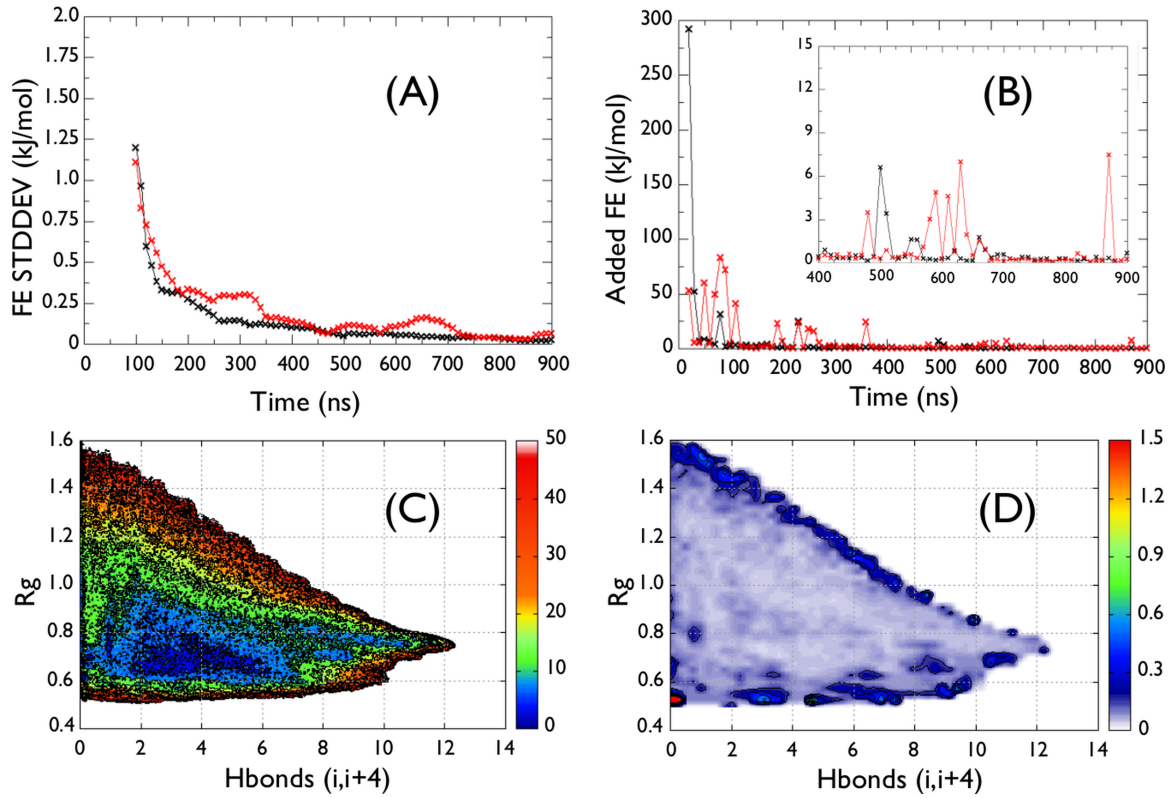

Figure S4: Convergence assessment of the Htt17_coil simulation. **(A)** Running average of the standard deviation of the 1D-FES (S_α in black and S_{gyr} in red) over 100 ns time-windows. **(B)** Total addition of free energy to the FES every 10 ns. **(C)** The 2D-FES (S_α;S_{gyr}) and **(D)** its uncertainty computed on the convergence interval (400–900 ns), which is determined from the small modifications of the FES after 400 ns shown in (A) and (B). We observe that the uncertainty on the FES is mostly located to its border, while it is low (< 0.5 kJ/mol) inside the basin. Energy isolines are drawn every 5 kJ/mol for **(C)** and 0.15 kJ/mol for **(D)**.

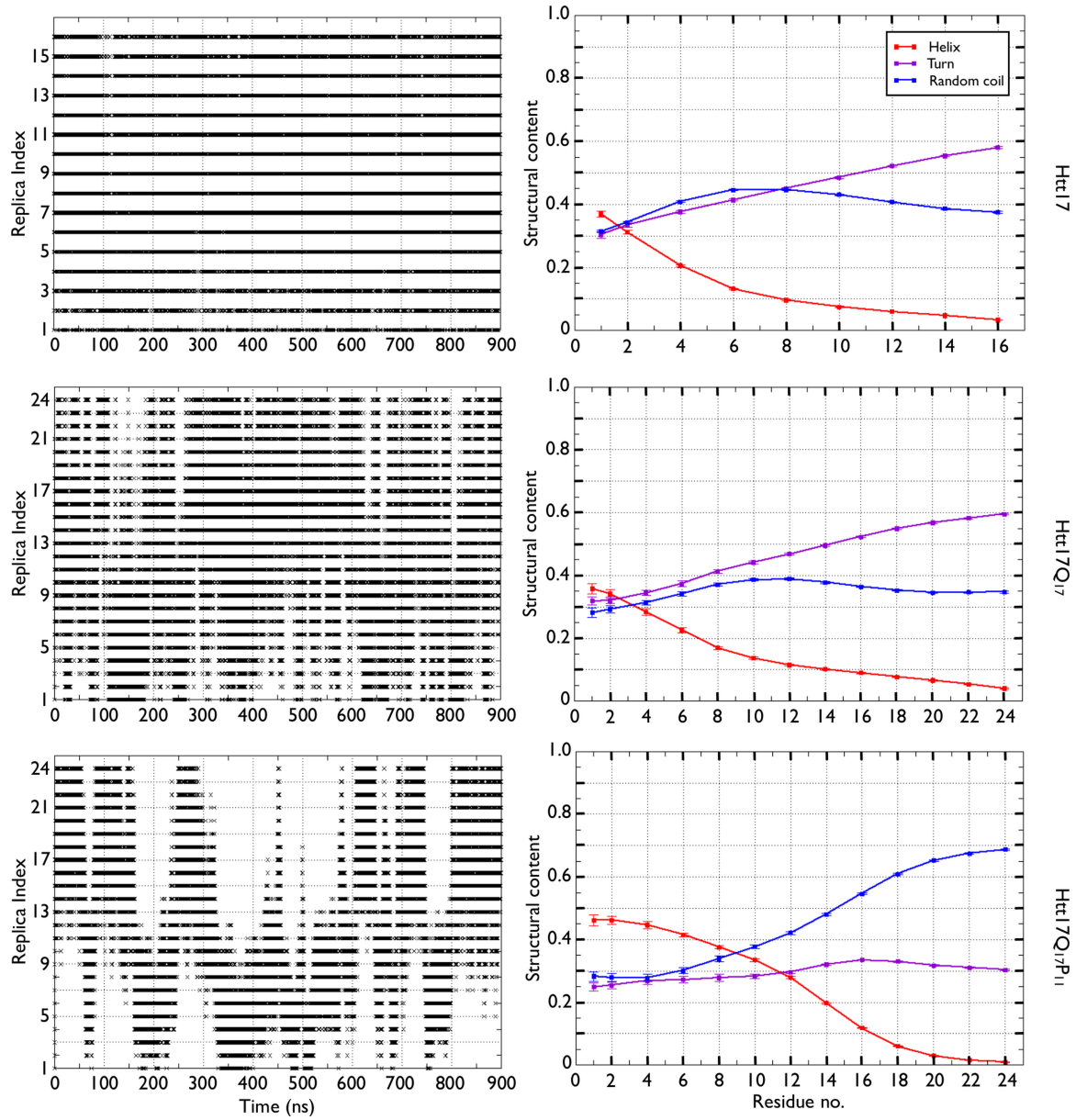

Figure S5: Sampling assessment of the HREX simulations. The left panel shows the replica index visiting the first scale. The right panel shows the secondary structure as a function of the scaling. Htt17Q_{17} and Htt17$Q_{17}P_{11}$ are respectively shown from top to bottom.

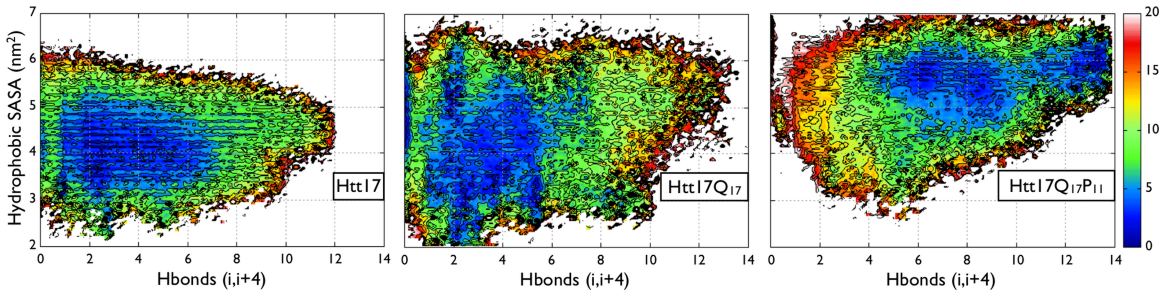

Figure S6: The FES of the Htt17 segment as a function of the number of helical H-bonds (S_α, horizontal axis) and SASA of Htt17's non-polar residues (vertical axis) is shown for Htt17, Htt17Q_{17} and Htt17$Q_{17}P_{11}$ from left to right. Energy isolines are drawn every 2 kJ/mol.

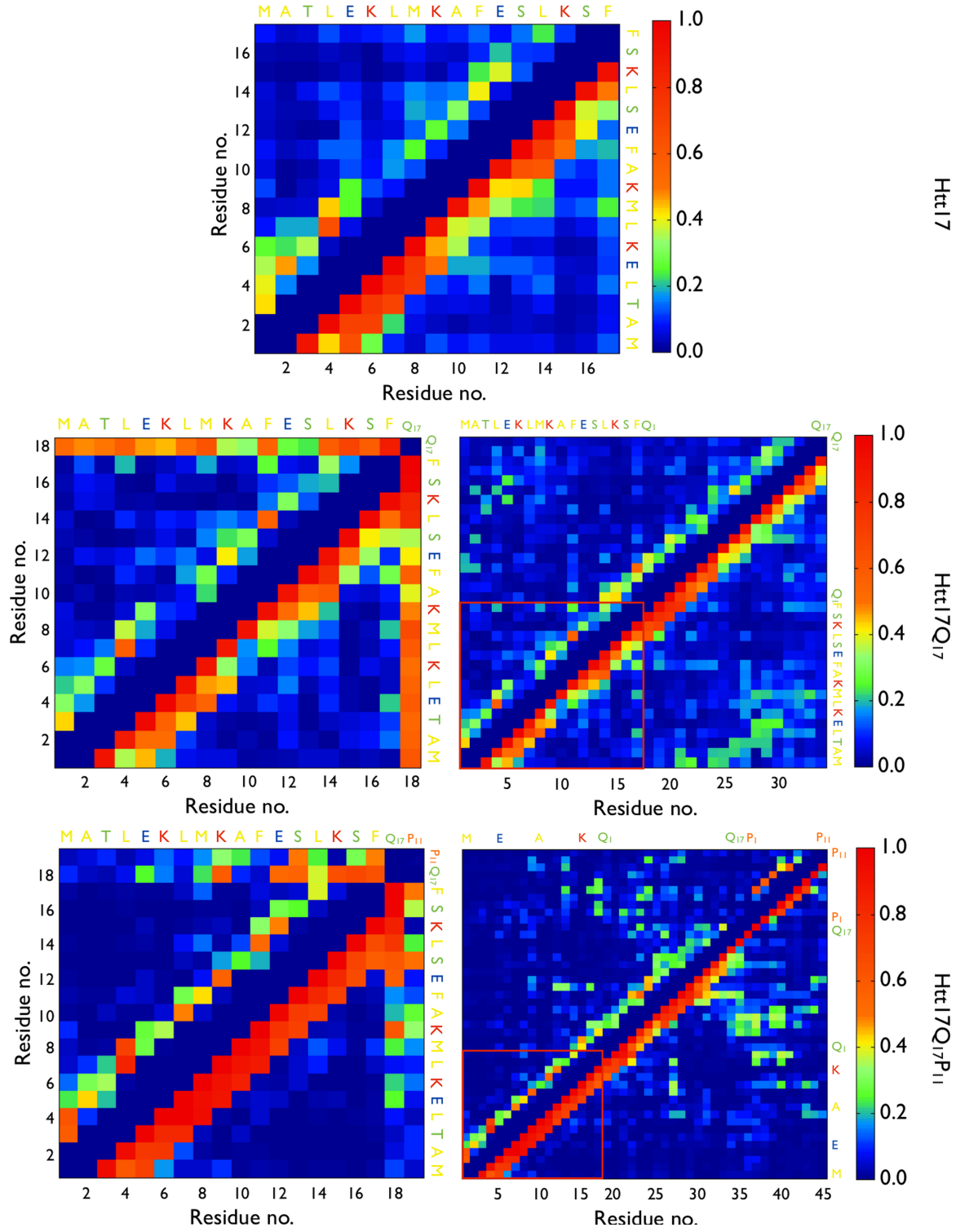

Figure S7: Contact maps of Htt17_nmr, Htt17Q_{17} and Htt17$Q_{17}P_{11}$ are shown from top to bottom. The side-chain/side-chain and the total number of contacts are respectively displayed on the upper and lower halves of the contact maps. For Htt17Q_{17} and Htt17$Q_{17}P_{11}$, the global propensity of Q_{17}/Htt17 and P_{11}/Htt17 contacts (left column) and the per residue probability of each individual glutamines and prolines (right column) are shown. The red square indicates the Htt17/Htt17 contacts when appropriate.

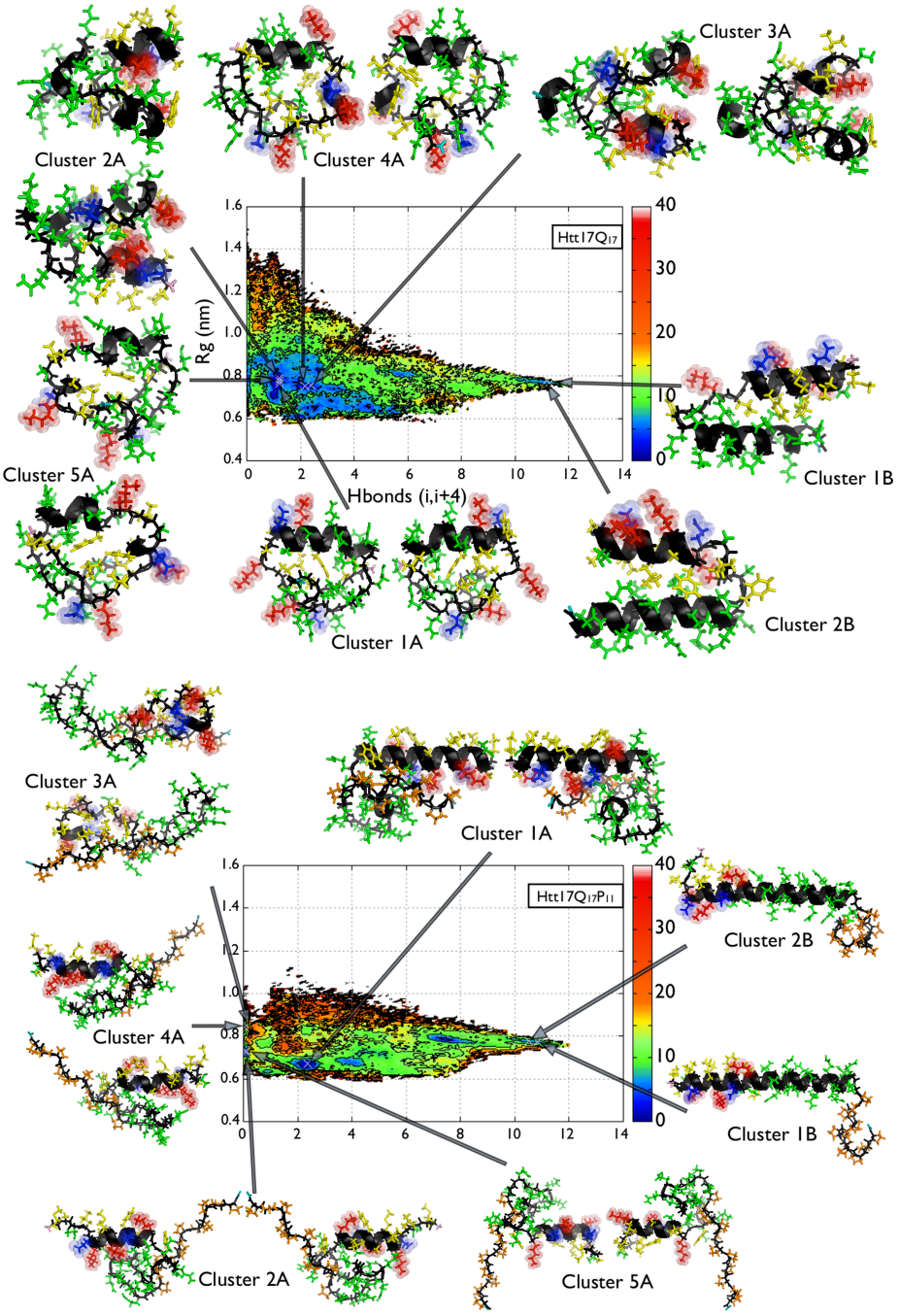

Figure S8: The FES of the Q_{17} segment as a function of the number of helical H-bonds (S_α, horizontal axis) and gyration radius (S_{gyr}, vertical axis) is shown for Htt17Q_{17} (top) and Htt17$Q_{17}P_{11}$ (bottom). The main clusters of the conformations inside the main basin (below 4 kJ/mol) and those with more than 9.5 helical H-bonds (below 8 kJ/mol) are displayed around the FES. Energy isolines are drawn every 4 kJ/mol.

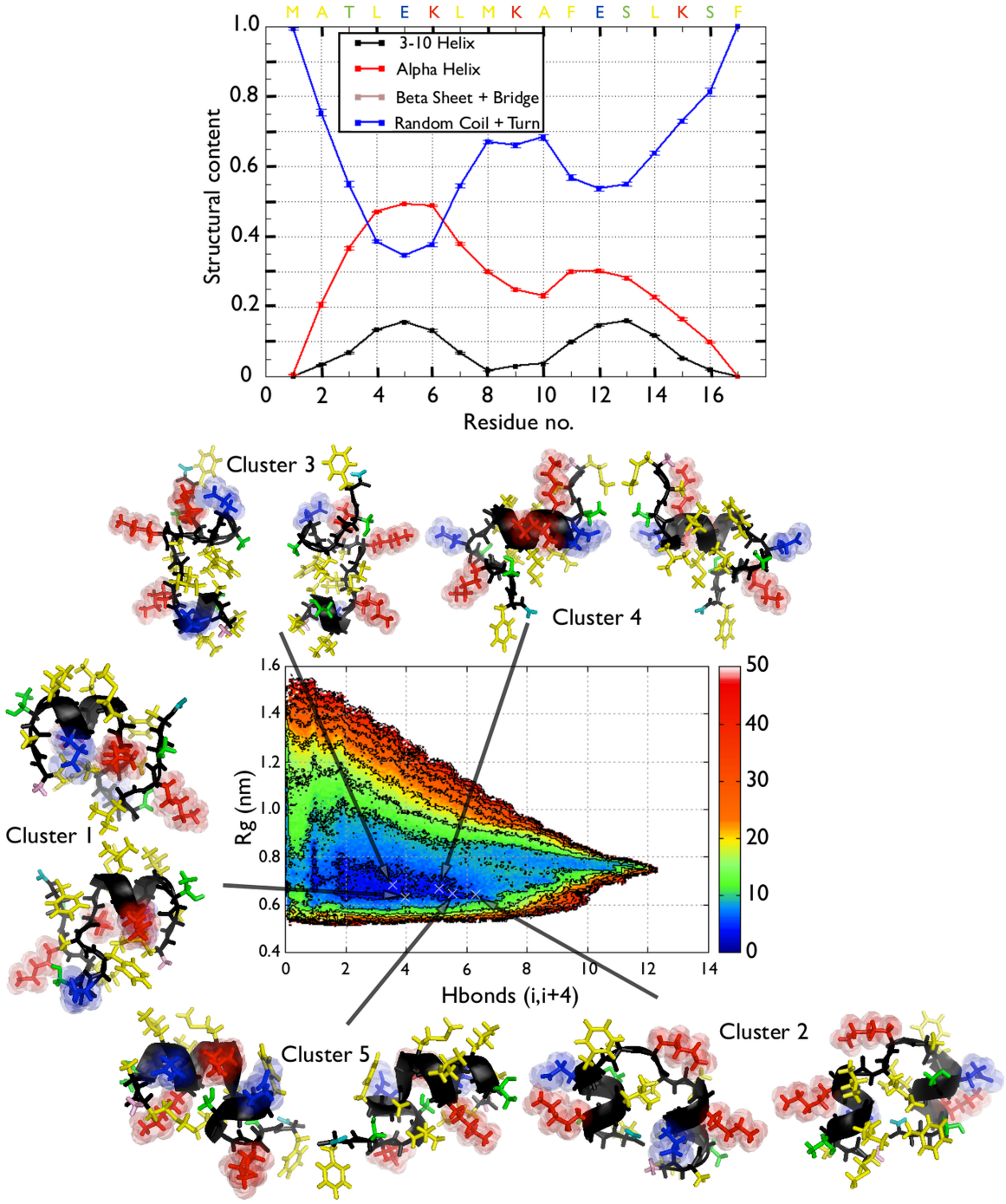

Figure S9: The per residue secondary structure of Htt17 from the HREXMetaD simulation starting from the random structure is shown in the top panel. The probability of α-helix, 3-10 helix, β-bridge and β-strand, and all other motifs are respectively shown in red, black, brown and blue. The FES of the Htt17 segment as a function of the number of helical H-bonds (S_α, horizontal axis) and gyration radius (S_{gyr}, vertical axis) is shown in the bottom panel. Energy isolines are drawn every 5 kJ/mol. The FES is surrounded by the cluster center of the representative structures found below 5 kJ/mol.

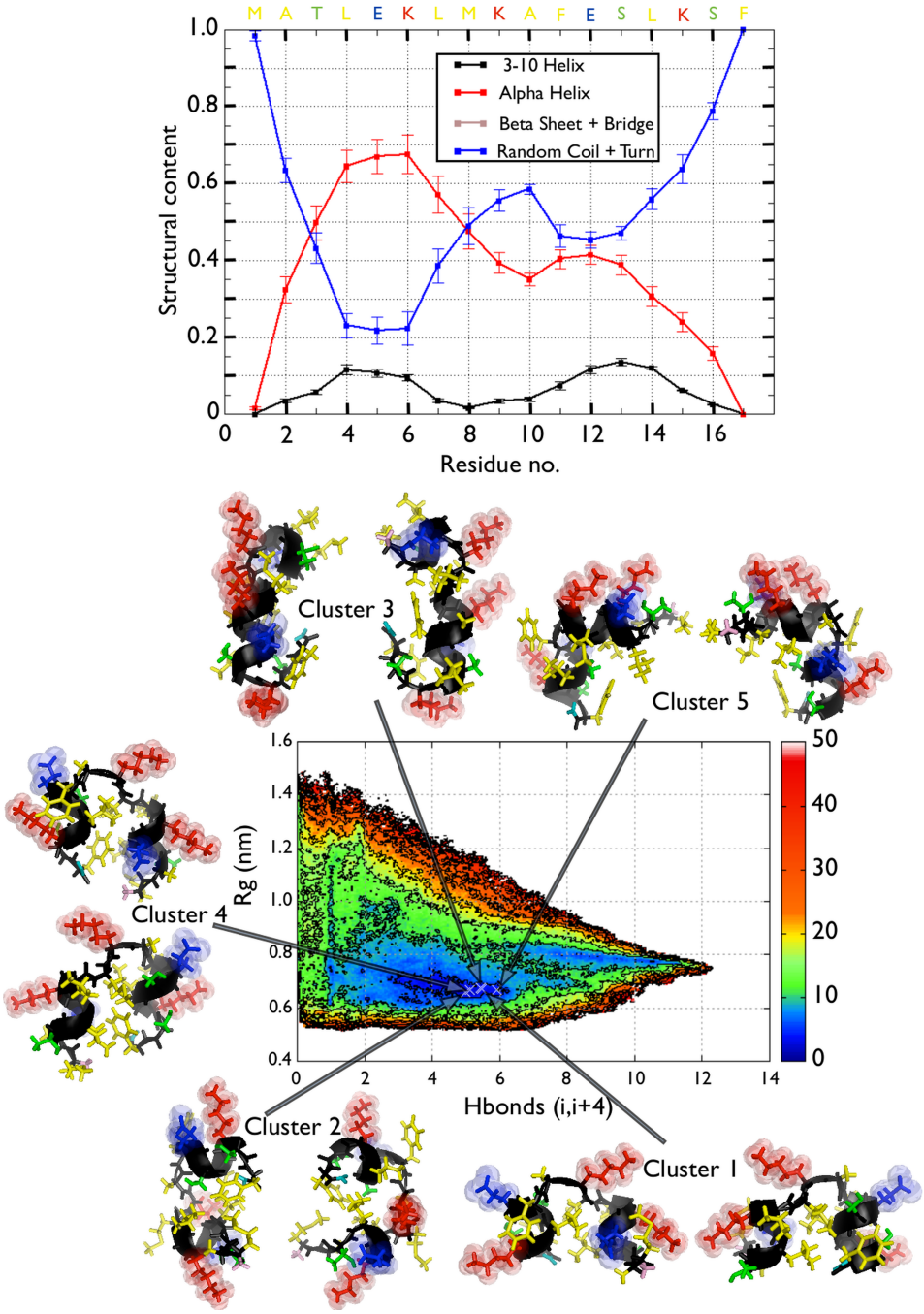

Figure S10: The per residue secondary structure of Htt17 from the PTMetaD simulation starting from a random coil structure is shown in the top panel. The probability of α-helix, 3-10 helix, β-bridge and β-strand, and all other motifs are respectively shown in red, black, brown and blue. The FES of the Htt17 segment as a function of the number of helical H-bonds (S_α, horizontal axis) and gyration radius (S_{gyr}, vertical axis) is shown in the bottom panel. Energy isolines are drawn every 5 kJ/mol. The FES is surrounded by the cluster center of the representative structures found below 5 kJ/mol.

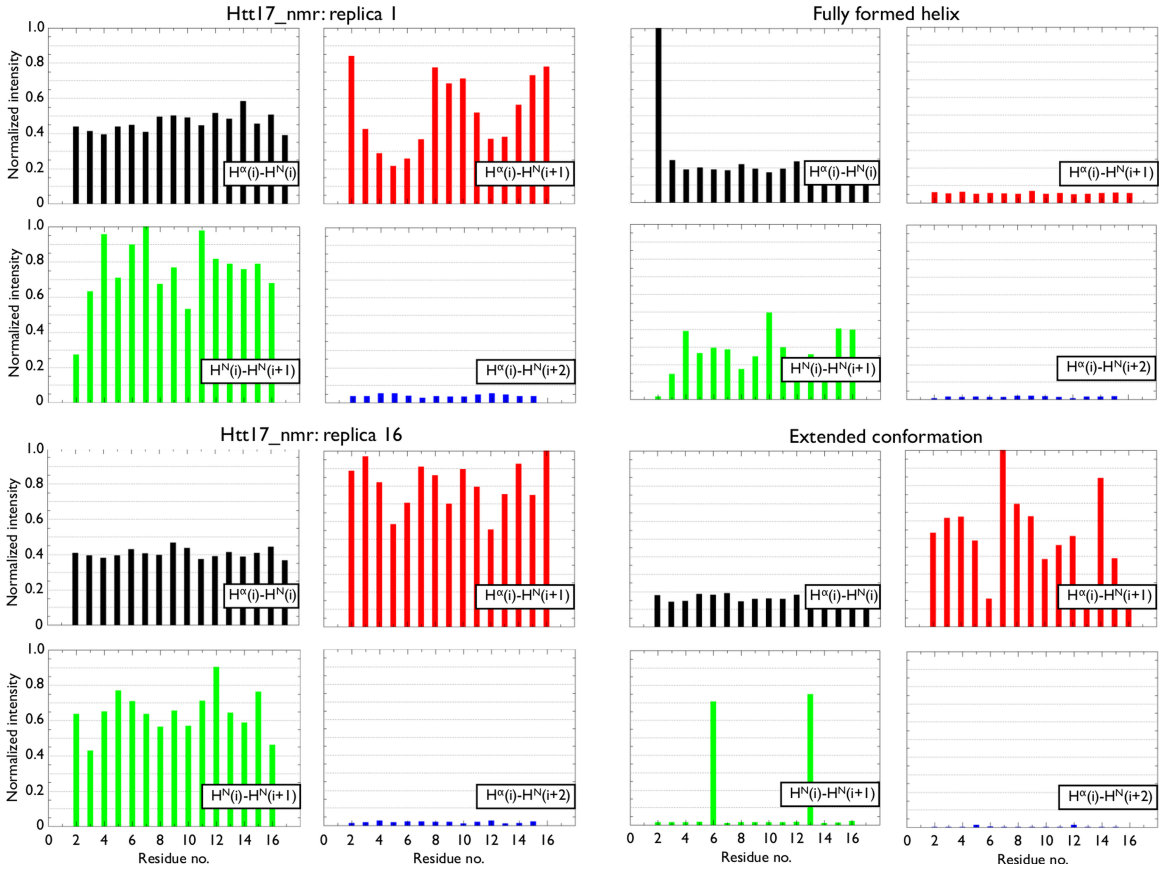

Figure S11: The computed intensities of the interproton NOEs for all residues between the H^{α} of residue i and the H^{N} of residues i, i+1 and i+2, as well as between the H^{N} of residues i and i+1. The top left panel shows the NOEs for the analysis replica, the bottom left panel shows the NOEs for the most scaled replica, the top right panel shows the NOEs of a fully formed α-helix and the bottom right panel shows the NOEs of a fully extended conformation.

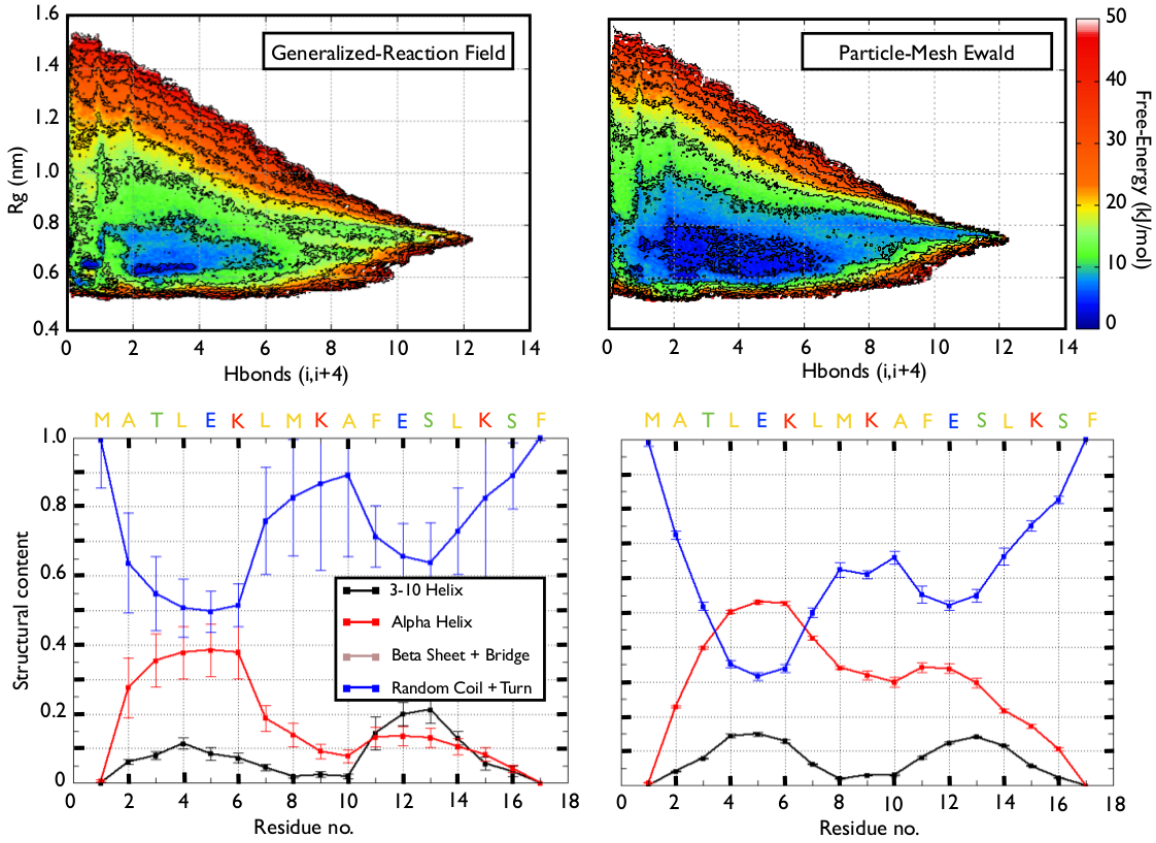

Figure S12: The FES (shown in the top row) and secondary structure profile per residue (shown in the bottom row) of Htt17 using a Generalized-Reaction Field (shown in the left column) or the Particule-Mesh Ewald scheme (shown in the right column). The probability of α-helix, 3-10 helix, β-bridge and β-strand and turn/coil are respectively shown in red, black, brown, and blue. The vertical black dotted lines indicate respectively the end of the Htt17 segment and the end of the Q_{17} segment.

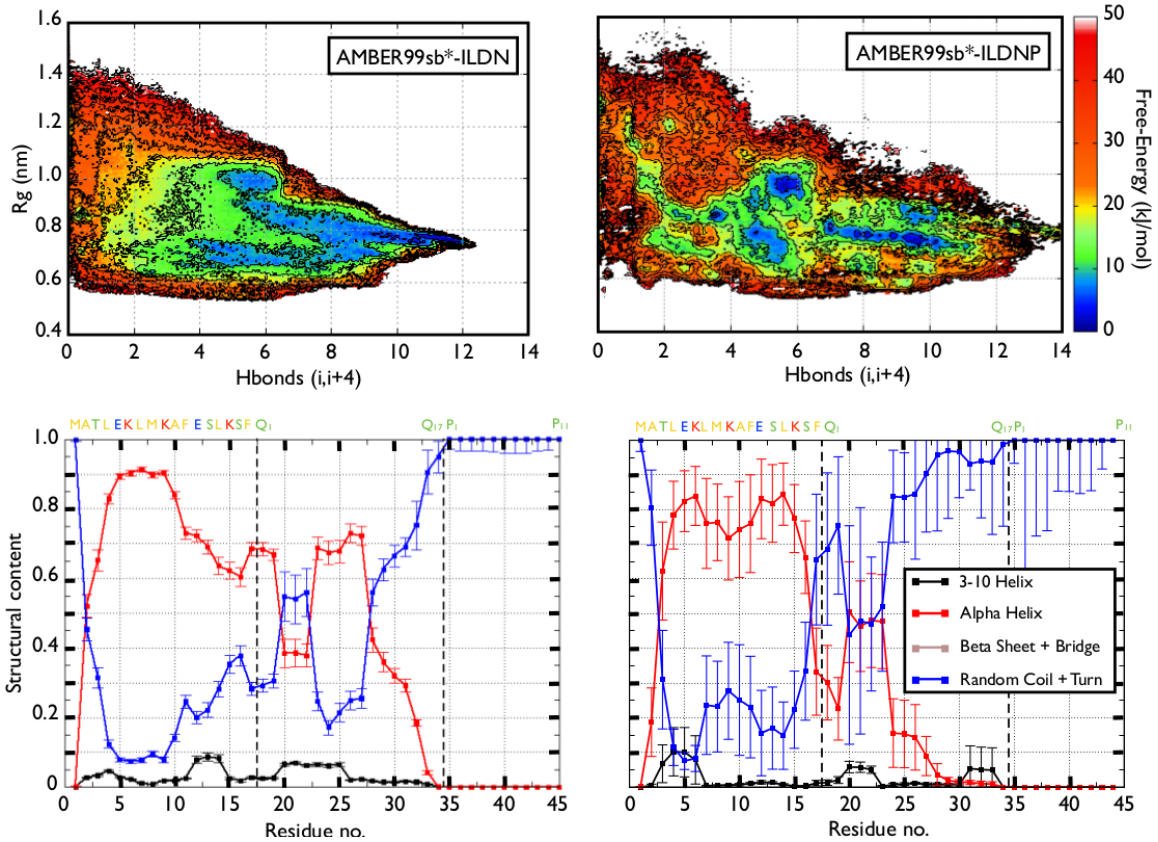

Figure S13: The FES (shown in the top row) and secondary structure profile per residue (shown in the bottom row) of Htt17$Q_{17}P_{11}$ using the AMBER99sb*-ILDN forcefield (shown in the left column) or the AMBER99sb*-ILDNP forcefield, with the improved proline parameters (shown in the right column). The probability of α-helix, 3-10 helix, β-bridge and β-strand and turn/coil are respectively shown in red, black, brown, and blue. The vertical black dotted lines indicate respectively the end of the Htt17 segment and the end of the Q_{17} segment.

List of Figures